Performance Based Earthquake Engineering: Application to an Actual Bridge-Foundation-Ground System

Joel P. Conte[I], Yuyi Zhang[II]
[I]*Department of Structural Engineering, University of California at San Diego, La Jolla, California 92093-0085*
[II]*Anatech Corporation, 5435 Oberlin Drive, San Diego, California 92121*

Keywords: Bridge-foundation-ground system, probabilistic performance assessment, seismic hazard analysis, seismic demand analysis, fragility analysis, reliability analysis, seismic loss analysis

SUMMARY:
Performance-based earthquake engineering (PBEE) is emerging as the next-generation design and evaluation framework under which new and existing structures will be analyzed for seismic adequacy. This paper presents the application of the PBEE methodology developed at the Pacific Earthquake Engineering Research (PEER) Center to the Humboldt Bay Middle Channel (HBMC) Bridge modeled and analyzed as a nonlinear soil-foundation-structure interaction (SFSI) system. The HBMCB, with precast and prestressed concrete I-girders and cast-in-place concrete slabs, is fairly representative of older AASHTO-Caltrans girder bridges. It is supported on pile groups in soils potentially vulnerable to liquefaction during an earthquake, which could induce lateral spreading and permanent soil deformations.
This paper presents the nonlinear finite element model of the bridge-foundation-ground (BFG) system used in this study and then focuses on the several analytical steps of the PEER PBEE methodology as applied to this bridge. This methodology integrates in a probabilistic framework seismic hazard analysis, seismic demand analysis, capacity analysis, reliability/damage analysis, and loss analysis. Several potential failure mechanisms of the HBMC Bridge are considered: flexural failure of bridge piers, failure of shear key(s), and unseating. For each failure mechanism, several limit/damage-states measuring the stage of formation of the mechanism are defined. The seismic reliability against these limit-states is evaluated in terms of mean annual rate/frequency of exceedance or, alternatively, return period. As outcome of seismic loss analysis, the seismic loss hazard curve expresses the mean annual frequency of exceeding any total annual seismic repair/replacement cost. The paper presents selective results illustrating the various steps of the PEER PBEE methodology as applied to the HBMC Bridge.

1 INTRODUCTION

Seismic reliability analysis of actual structures is a very challenging task due to the large number of factors affecting structural seismic demand and capacity and the uncertainties associated with these factors. Uncertainties in the predicted seismic demand emanate from the basic uncertainties characterizing the seismic source (e.g., fault rupture mechanism, occurrence in space and time, magnitude), the wave propagation path, the local soil conditions, the ground motion time histories at the support points (foundation) of the structure, the properties of the structure itself, and the various methods/models used to predict each of the above ingredients of the earthquake engineering problem from the source parameters to the seismic response/demand of the structure. Generally, structural capacity terms depend on cyclic material properties, geometric properties of structural members, system configuration and methods/models used to predict the capacity. Over the last few decades, a significant body of research has been performed to develop various ingredients of a general methodology to evaluate the seismic reliability of structures accounting for all pertinent sources of uncertainty mentioned above (e.g., Kennedy et al. 1980, Tzavelis and Shinozuka 1988, Esteva and Ruiz 1989, Wen 1995, Song and Ellingwood 1999, Cornell et al. 2002, Yun et al. 2002).

The Pacific Earthquake Engineering Research (PEER) Center, funded by the U.S. National Science Foundation, has focused for a number of years on the development of procedures, knowledge and tools for a comprehensive probabilistic seismic performance assessment methodology, referred to as the PEER PBEE methodology, for building and bridge

structures (Cornell and Krawinkler 2000, Porter 2003, Moehle and Deierlein 2004). This paper presents the analysis of the Humboldt Bay Middle Channel (HBMC) Bridge testbed (see Fig. 1) based on the PEER PBEE methodology.

The HBMC Bridge, designed in 1968 and built in 1971, is located near Eureka in northern California. It is fairly representative of older AASHTO-Caltrans girder bridges built under the dated elastic design philosophy, before ductile detailing was common. This nine span bridge structure is 330-meter long, 10-meter wide, and 12-meter high. The superstructure consists of four precast prestressed concrete I-girders and cast-in-place concrete slabs. It is supported by two seat-type abutments and eight single pier bents with cap beam founded on pile group foundations. The superstructure is continuous over Piers # 1, 2, 4, 5, 7 and 8 and has expansion joints at both abutments and on top of Piers # 3 and 6. At these expansion joints, there are shear keys with gaps on both sides, while at the continuous joints, a shear key with # 4 dowels connects the superstructure to the pier bent. Thus, the bridge structure consists of three frames interconnected through shear keys with gaps at the two interior expansion joints. Piers # 3, 4, 5, 6 and 7 are supported on five 54-inch diameter driven precast, prestressed concrete piles, while Piers # 1, 2, 8 and the abutments are founded on sixteen (4 rows of four) 14-inch driven precast, prestressed concrete square piles.

Figure 1. Humboldt Bay Middle Channel Bridge (Courtesy of Caltrans): (a) aerial view, (b) superstructure

The river channel has an average slope from the banks to the center of about 7 percent (4 degrees). The foundation soil consists mainly of dense fine-to-medium sand (SP/SM), organic silt (OL), and stiff clay (OL) layers, with thin layers of loose and soft clay (OL/SM) located near the ground surface. This site is considered vulnerable to liquefaction under strong ground shaking. Soil liquefaction, approach fill settlement and soil lateral spreading are issues of interest in this bridge testbed.

The HBMC Bridge was the object of two Caltrans (California Transportation Department) seismic retrofit efforts completed in 1995 and 2005, respectively. The objectives of the first retrofit were to mitigate the potential for unseating and diaphragm damage and to strengthen the shear keys by enlarging and reinforcing the superstructure. The objective of the second retrofit was to strengthen the substructure (piers, pile caps, and pile groups) (Zhang et al. 2007a).

2 COMPUTATIONAL MODEL OF BRIDGE-FOUNDATION-GROUND SYSTEM

A two-dimensional nonlinear finite element model (Fig. 2) of the HBMC Bridge in its "as-built" condition, including the superstructure, piers, pile group foundations, abutments, embankment approaches, and foundation soil, was developed in the software framework OpenSees (Mazzoni et al. 2005), the PEER analytical platform for seismic response simulation of structural and/or geotechnical systems. This study considers the seismic response of the bridge in the longitudinal direction only.

Within each span, the four I-girders are idealized as a single equivalent linear elastic beam-column element, since due to the design of the piers, material yielding cannot spread into the superstructure. Each bridge pier is modeled via a single force-based, fiber-section beam-column element with five Gauss-Lobatto (G-L) points along its length. The cross-sections at the five G-L points are discretized into fibers of confined concrete (core), unconfined concrete (cover) and reinforcing steel (Fig. 3). The uni-axial Kent-Scott-Park constitutive model (Fig. 4) with degraded linear unloading/reloading stiffness and no tensile strength is employed to model the concrete material, with f_c' = compressive strength, ε_c' = strain at peak strength, f_{cu}' = residual (crushing) strength, ε_{cu}' = strain corresponding to f_{cu}'. For the upper four G-L points of each pier, the uni-axial bilinear material model (or uni-axial J_2 plasticity model with linear kinematic hardening) is used to model the reinforcing steel with the parameters E_s = Young's modulus, f_y = yield strength, and b = post-yield hardening ratio. At the base of the eight piers, all the longitudinal reinforcing bars are lap spliced. The uni-axial tri-linear hysteretic material model shown in Fig. 5 is used to model the reinforcing steel in the lap-spliced region (i.e., bottom G-L point). The material properties for this hysteretic material model were calibrated based on the envelope of the lateral force-deformation (drift) response of the bridge piers as predicted using a mechanics-based model of lap spliced columns, itself calibrated with experimental data. Figs. 6 and 7 show the cyclic moment-curvature response of the

pier fiber-sections defined at the upper four G-L points and at the bottom G-L point, respectively. Fig. 8 displays the moment-curvature response at the four lower G-L points of a cantilever pier subjected to monotonic pushover. It is seen that the plastic deformations (with softening) concentrate at the base G-L point, while the other G-L points undergo quasi-elastic loading and elastic unloading.

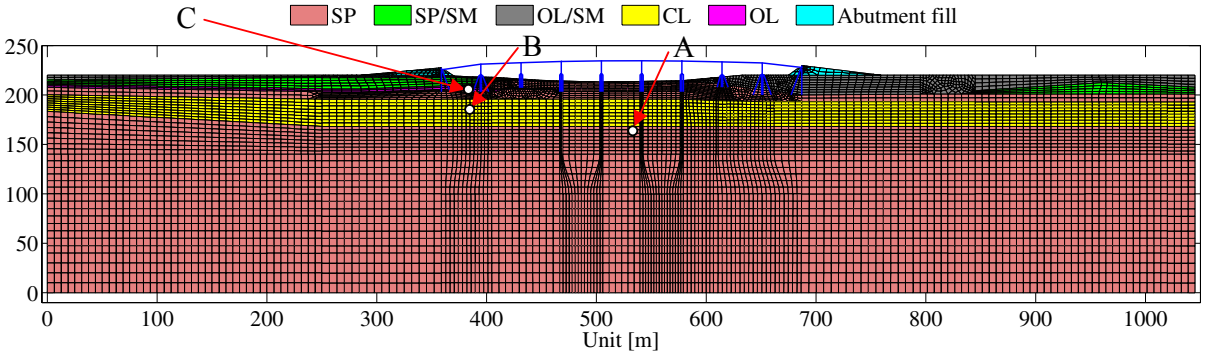

Figure 2. OpenSees finite element model of HBMC bridge-foundation-ground system

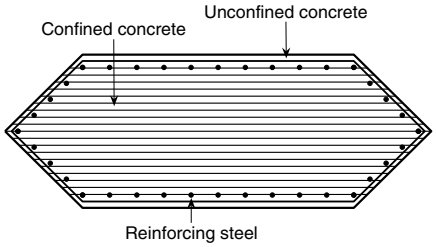

Figure 3. Fiber discretization of pier cross-section

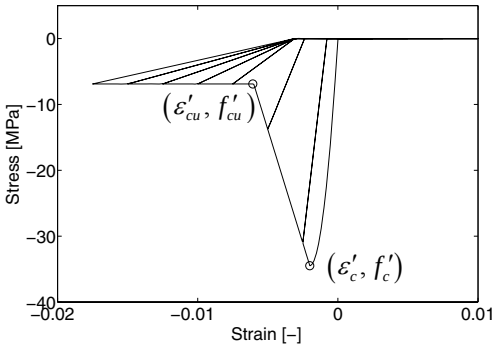

Figure 4. Uni-axial cyclic Kent-Park-Scott concrete model

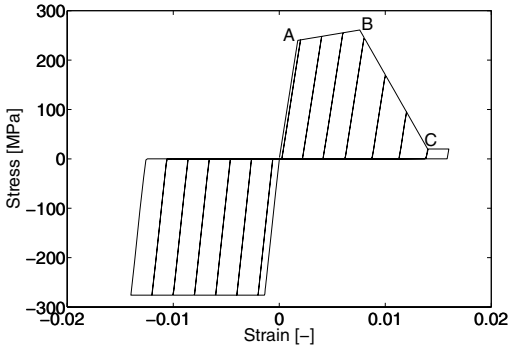

Figure 5. Uni-axial hysteretic model for reinforcing steel in the lap spliced region

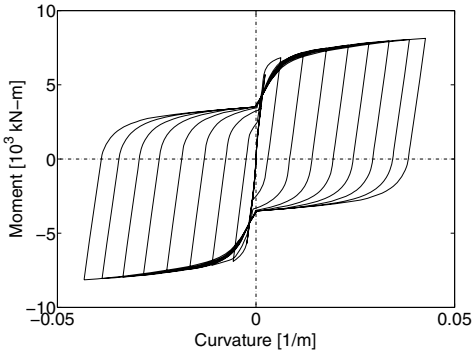

Figure 6. Cyclic moment-curvature response of fiber-section at four upper G-L points of pier elements

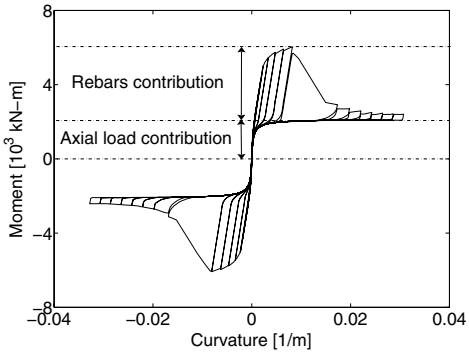

Figure 7. Simulated cyclic base moment-curvature response of lap-spliced pier

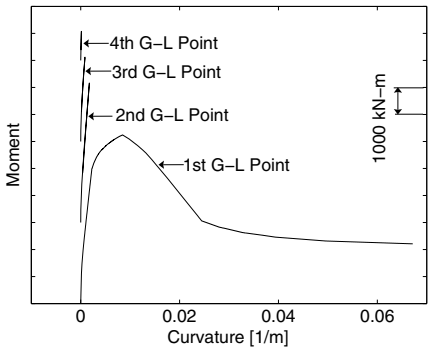

Figure 8. Moment-curvature responses at four lower G-L points of cantilever bridge pier subjected to pushover

Each out-of-plane row of piles is lumped into a single equivalent pile with a monolithic cross-section defined by the union of the cross-sections of the piles in that row and following Bernoulli-Euler beam theory. Each lumped pile is then discretized into a number of force-based, fiber-section beam-column elements. The pile nodes are directly connected to the surrounding soil nodes in the translational degrees of freedom. Thus, the effects of slippage and friction between soil and piles and/or pile-soil separation (gapping) near the ground surface are not accounted for in this study. Pile caps are also modeled using force-based, fiber-section beam-column elements.

At the abutment (expansion) joints, interior expansion joints and continuous joints, the superstructure is connected to the abutments and pier bents through shear keys in the longitudinal direction. Fig. 9 illustrates the FE modeling of an interior expansion joint. The shear keys are modeled using zero-length elements with an aggregated uni-axial material model composed of an "elastoplastic material model with gap", an "elastoplastic material model with hook" and another elastoplastic material model, all configured in parallel. The purpose of the last elastoplastic material model is to represent the friction between the superstructure and the bridge pier. In order to simulate the physical fracture of shear keys, an ultimate deformation is specified for each shear key aggregated material model so that its internal force drops to zero when this deformation is reached and remains zero thereafter. Fig. 10 shows a typical cyclic force-deformation response of a shear key.

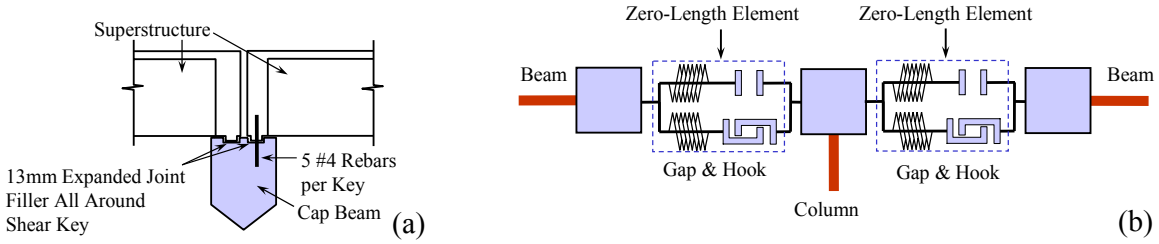

Figure 9. Shear key at interior expansion joints: (a) as built, and (b) FE model

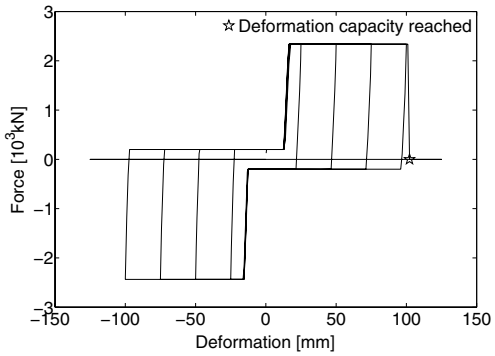

Figure 10. Typical cyclic force-deformation response of shear keys

The soil domain is assumed under plane strain condition. It extends 1050*m* in length and 220*m* in depth, at which level bedrock is encountered. The abutment fill is modeled as dry material, while the other soil layers, which are below the water table (near the ground surface), are modeled as saturated materials. The soil domain is spatially discretized using four-noded, bilinear, isoparametric elements with four integration points each. The materials in the various soil layers are modeled using pressure dependent (e.g., sand) or pressure independent (e.g., clay) effective-stress multi-yield-surface plasticity models, see Fig. 11. To simulate undrained response in saturated soil layers, the above material models of solid phase are embedded in a linear elastic material model with high bulk modulus to model the fluid phase. The most significant soil material parameters are the friction angle, cohesion, and initial (low strain) shear modulus. Fig. 12 shows a comparison of the shear wave velocity profile measured (0.25 mile north-west of the west abutment of the HBMC Bridge) and represented by the FE model.

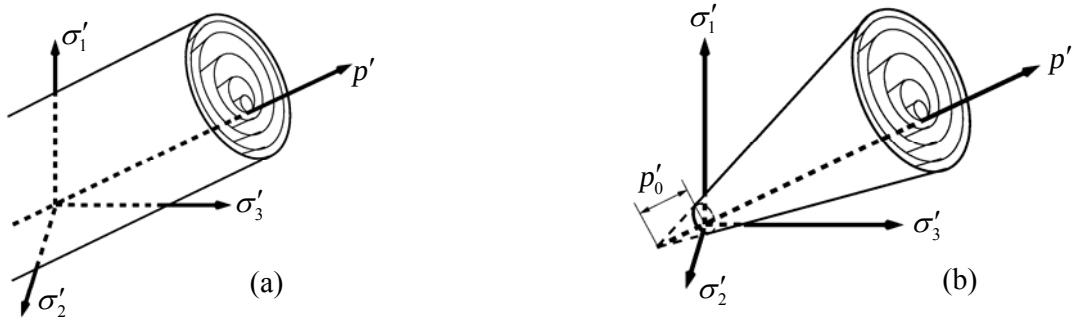

Figure 11. Multi-yield surface soil plasticity models: (a) clay type soils (pressure-independent), (b) sand type soils (pressure-dependent)

The bedrock underlying the computational nonlinear soil domain is modeled as a homogeneous, linear elastic, undamped semi-infinite half-space. The incoming seismic waves in the bedrock are as-

sumed to be vertically propagating shear waves. Lysmer-type absorbing (transmitting) boundaries are incorporated in the FE model so as to avoid spurious wave reflections along the boundaries of the computational soil domain.

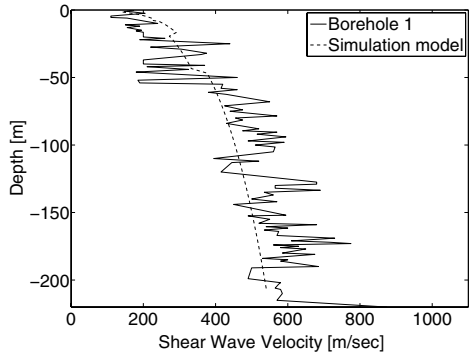

Figure 12. Shear wave velocity profile

Consistent with the above assumptions, the seismic input is defined as equivalent nodal forces, which are proportional to the (soil particle) velocity of the incident seismic wave, applied in the horizontal direction along the base of the computational soil domain. Seismic inputs, however, are usually expressed in terms of accelerograms recorded at the free-field ground surface. Consequently, the free-field motion considered needs to be deconvolved in order to obtain the corresponding incident wave motion at the base of the computational soil domain. In this study, SHAKE91 (Idriss and Sun 1993) was used to deconvolve iteratively the free field surface motions to the base of the computational soil domain through the various soil layers modeled with equivalent linear soil properties. The latter are obtained based on the effective shear strain in each layer and the shear modulus reduction and damping curves.

To simulate the seismic response of the FE model of the HBMC Bridge described above, a five-stage analysis procedure is used in order to apply the gravity loads to the soil first, then to the bridge, and then apply the seismic excitation, with change of material constitutive model and boundary conditions of the soil domain between stages. For further details on the FE model described above, the interested reader is referred to (Zhang et al. 2007a).

Based on small amplitude vibration analysis of the above FE model of the HBMC bridge-foundation-ground system, the natural frequencies of the two lowest system vibration modes with participation from both the soil and the bridge structure are found to be: $T_I = 0.71$sec and $T_{II} = 0.59$sec.

Figs. 13-16 present some selective simulation results obtained from the FE model presented above when subjected to the fault-parallel component of the 1985 Valparaiso, Chile earthquake recorded at Pichilemu station scaled to match the 5% damped elastic spectral acceleration at $T_I = 0.71$sec corresponding to a probability of exceedance of 2% in 50 years (return period = 2,475 years).

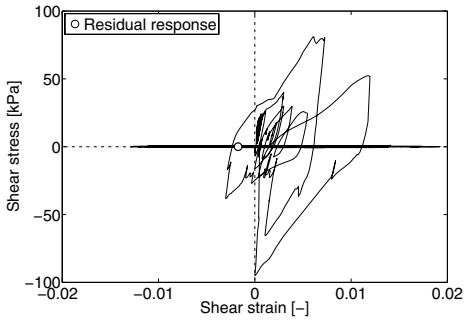

Figure 13. Shear stress vs. shear strain response at soil location C (see Fig. 2).

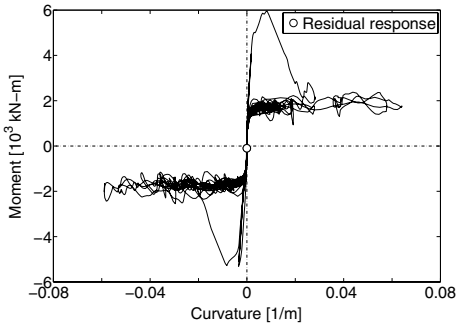

Figure 14. Moment-curvature response at the base cross-section of Pier # 3

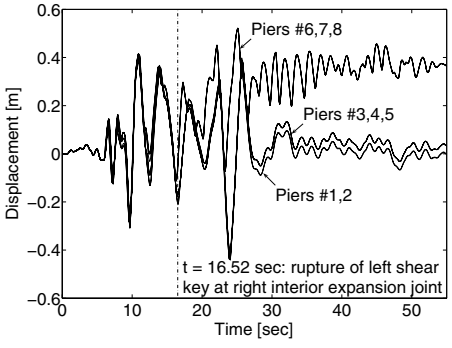

Figure 15. Total horizontal displacement histories of all pier bases

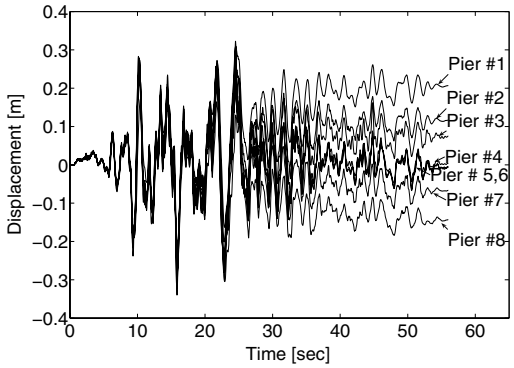

Figure 16. Total horizontal displacement histories of all pier tops

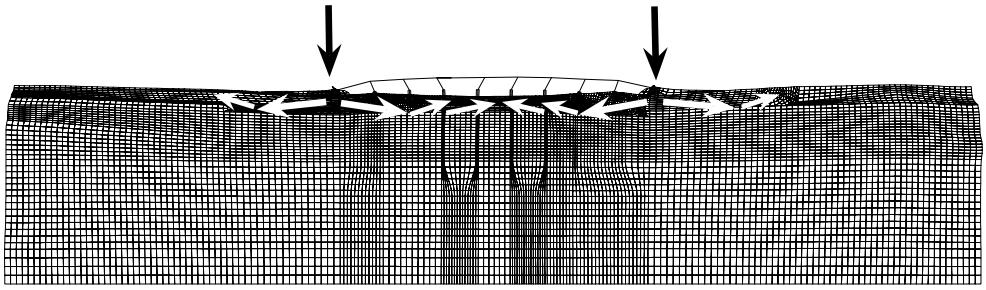

Figure 17. Deformed FE mesh at the end of the earthquake (exaggerated scale)

Fig. 13 shows the shear stress vs. shear strain hysteretic response in the soil at location C (see Fig. 2) where the soil reaches liquefaction during the earthquake, resulting in dramatic stiffness degradation and strength deterioration. As can be seen from Fig. 14 which shows the moment-curvature response at the base cross-section of Pier # 3, the lap-spliced failure mechanism is fully developed during the earthquake. The total horizontal displacement response histories of the top and base of all eight bridge piers are shown if Figs. 15 and 16, respectively. After a shear key failure at the right expansion joint, the right frame of the bridge undergoes significant horizontal displacement relative to the other two frames still closely connected (see Fig. 15). From Fig. 16, it is observed that the base of each pier moves progressively and permanently towards the center of the river channel due to soil lateral spreading induced by reduction in soil strength caused by build-up of pore water pressure in cohesionless soil layers during the earthquake. The deformed FE mesh of the BFG system at the end of the earthquake is displayed in Fig. 17 in exaggerated scale. Severe damage to bridges caused by similar pattern of lateral spreading has been observed in previous earthquakes (e.g., Kramer 1996, Figures 1.8 and 1.9). According to these simulation results, the seismic response of the bridge in its longitudinal direction is mostly driven by the nonlinear inelastic response of the underlying soil. The presence of the bridge structure was found to have little influence on the seismic response of the foundation soil. The plastic soil deformations impose large residual deformations and internal forces on the bridge structure after the earthquake.

3 FAILURE MECHANISMS, LIMIT-STATES AND ASSOCIATED ENGINEERING DEMAND PARAMETERS

Preliminary analyses and seismic response simulations revealed that pier flexural failure at the base (in the spliced region), unconfined shear key failure, and unseating at the abutments and interior expansion joints are the critical failure mechanisms for the HBMC Bridge. Each of these failure mechanisms has been observed in previous earthquakes as shown in Fig. 18.

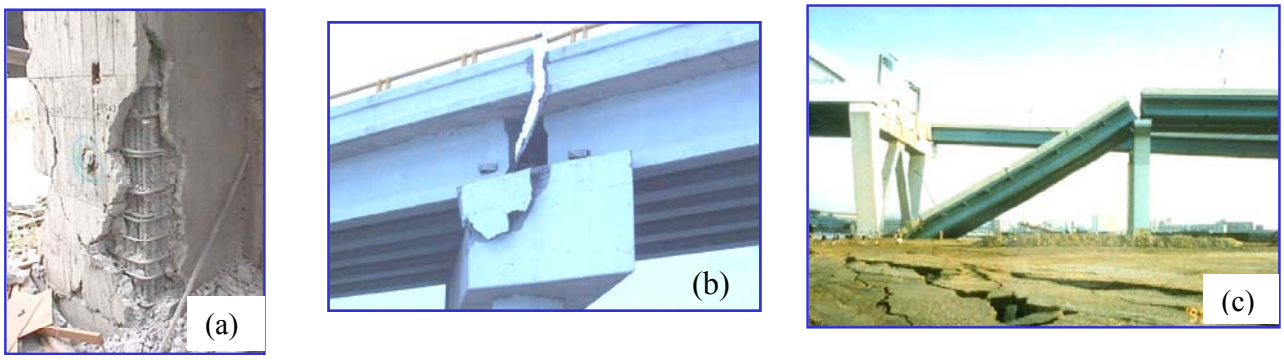

Figure 18. Critical bridge failure mechanisms observed in past earthquakes: (a) pier flexural failure in spliced region, (b) unconfined shear key failure, (c) unseating

For each of the three failure mechanisms considered, five discrete stages of formation of the mechanism, called limit-states (LSs), are considered. These performance-based limit-states are defined as follows (Hose and Seible 1999): I - cracking, II - yielding, III - formation (initiation) of the mechanism (when peak capacity is reached), IV - full formation of mechanism, and V - strength degradation (collapse). The selection of these five limit-states by Hose and Seible was based on field investigations following seismic events, detailed assessment of laboratory experiments and comprehensive analyses. These five limit-states relate explicitly to the component/structure capacity.

Pier Flexural Failure Mechanism. Fig. 19 illustrates the five limit-states of a pier failing in flexure in the lap-spliced region (Hose and Seible 1999). The peak lateral (or tangential) pier drift Δ, defined

as the relative top-to-bottom horizontal displacement of the pier, minus the horizontal displacement at the top due to a rigid body rotation equal to the rotation of the base, is selected as the Engineering Demand Parameter (*EDP)* for pier flexural failure in the lap-spliced region. The five limit-states for the pier flexural failure mechanism are marked in Fig. 20 which represents the analytically predicted base shear versus lateral drift response of a typical pier (average height of 12*m*) of the HBMC Bridge. It was found that within the range of the varying pier axial load ratio as determined by the earthquake response simulations, limit-states III, IV and V occur at very close lateral drift values, indicating the brittle nature of this failure mechanism for the HBMC Bridge. Thus, only two limit-states are considered for this failure mechanism, namely limit-state II (yielding) and the joint limit-state III-IV-V (peak capacity and abrupt significant loss of flexural capacity).

(a) Limit-state I (b) Limit-state II (c) Limit-state III (d) Limit-state IV (e) Limit-state V

Figure 19. Pictorial description of limit-states of pier flexural failure in the lap-spliced region (Hose and Seible 1999)

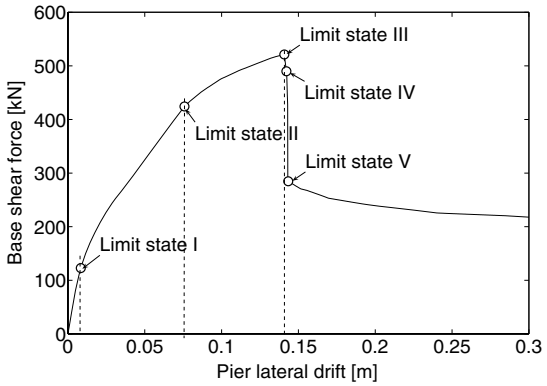

Figure 20. Limit-states for pier flexural failure mechanism

Shear Key Failure Mechanism. Simplified mechanistic capacity models (e.g., strut-and-tie model, Megally et al. 2001) predict that the (longitudinal) shear keys of the HBMC Bridge are also characterized by a brittle behavior, due to their low amount of steel reinforcement as well as the short anchorage length of the rebars specified in the "as built" drawings. For the shear key failure mechanism, the peak deformation across the weaker shear key in each pair is selected as an *EDP*. Simplified analytical predictions indicate that the limit-states I, II, and III for this failure mechanism fall within a very small deformation range. Therefore the five limit-states are reduced to joint LS-I-II-III, LS-IV and LS-V.

Superstructure Unseating Failure Mechanism. In the "as built" configuration of the HBMC Bridge, the bridge structure is separated into three frames by the interior expansion joints. Adjacent frames are connected only through shear keys at the expansion joints. As revealed by quasi-static push-over and dynamic analyses of the bridge, shear keys are very likely to yield and even rupture in the event of a strong earthquake. Unseating might occur at the abutment and interior expansion joints after the shear keys at these joints rupture and the relative displacement in the longitudinal direction between the bridge superstructure and its supports exceeds the corresponding seat width. For the unseating failure mechanism, only LS-V (collapse) is considered and the associated *EDP*, referred to hereafter as unseating displacement, is defined as the peak horizontal displacement of the superstructure away from its supports at both abutments and interior expansion joints.

In order to evaluate the seismic performance of the bridge system, the following system-level *EDPs* are defined for the three failure mechanisms considered: maximum peak lateral drift over all bridge piers (Δ^{P}), maximum peak shear key deformation at the abutments (Δ^{SK}_{abut}), interior expansion joints (Δ^{SK}_{exp}) and continuous joints (Δ^{SK}_{cont}), maximum peak unseating displacement at the abutments (Δ^{UNS}_{abut}) and at the interior expansion joints (Δ^{UNS}_{exp}). These system-level *EDPs* are used in the subsequent analysis to calculate the Mean Annual Rate (MAR) of the most critical component among a sub-group of similar components (e.g., piers, abutment shear keys, expansion joint shear keys, continuous joint shear keys, superstructure spans at the abutments and at the interior expansion joints) exceeding a specified limit-state for each of the three failure modes considered (i.e., pier lap-spliced flexural failure, shear key failure, superstructure unseating). Thus, each computed MAR of limit-state exceedance denotes the MAR that at least one of the components of a subgroup of similar components will exceed the specified limit-state for a given failure mode.

The PEER PBEE methodology breaks down the formidable task of predicting probabilistically the future seismic performance of a structure into four analytical steps (sub-tasks) integrated (coupled) using the Total Probability Theorem (TPT) (Ang and Tang 2007). These sub-tasks are: (1) probabilistic seismic hazard analysis, (2) probabilistic seismic demand

analysis, (3) probabilistic capacity analysis (fragility analysis), and (4) probabilistic loss analysis. Application of these four sub-tasks to the HBMC Bridge testbed are presented inn the Sections below.

4 PROBABILISTIC SEISMIC HAZARD ANALYSIS (PSHA)

In order to derive an expression for the MAR of exceeding a limit-state or any particular value of a specified decision variable, it is necessary to define an earthquake random occurrence model in time. The homogeneous Poisson process is a reasonable model for this purpose (Cornell 1968). Let $N(t)$ denote the random number of earthquakes (of all magnitudes) that will occur in the next t years. According to the Poisson model, given the MAR ν of occurrence of earthquakes (of all sizes), the probability that n earthquakes, $\{N(t)=n\}$, with random magnitudes and source-to-site distance will occur in t years is given by

$$P_{N(t)}(n,t)=\frac{(\nu t)^n \exp(-\nu t)}{n!} \qquad n=0,1,2,\ldots \tag{1}$$

The Poisson process has an important property: if a random selection is made from a Poisson process with mean rate λ such that each occurrence is selected with probability p, independently of the others, the resulting process is also a Poisson process, called Censored Poisson process, with a mean rate $p\lambda$ (Benjamin and Cornell 1970). In this study, the objective of PSHA is to compute for the HBMC Bridge site the annual probability of exceeding any particular value of a specified ground motion intensity measure (IM) taken as the 5% damped elastic spectral acceleration at the first (low amplitude vibration) period, $S_a(T_1 = 0.71\text{sec}, \xi = 5\%)$, of the computational model of the bridge-foundation-ground system. For a given site, PSHA integrates the contributions of all possible seismic sources to calculate the MAR $\nu_{IM}(im)$ of Poisson random events $\{IM > im\}$ according to the TPT as

$$\nu_{IM}(im)=\sum_{i=1}^{N_{flt}}\nu_i \int_{R_i}\int_{M_i} P\left[IM>im \middle| M_i=m, R_i=r\right]\cdot f_{M_i}(m)\, f_{R_i}(r)\, dm\, dr \tag{2}$$

where N_{flt} = number of causative faults; ν_i = MAR of occurrences of earthquakes on fault (or seismic source) i. The functions $f_{M_i}(m)$ and $f_{R_i}(r)$ denote the probability density functions (PDF) of the magnitude (M_i) and source-to-site distance (R_i), respectively, given the occurrence of an earthquake on fault i. The conditional probability $P[IM > im \mid M_i = m, R_i = r]$ in Eq. (2), referred to as attenuation relationship (predictive relationship of IM given seismological variables M and R), is typically developed by applying statistical regression analyses to data either recorded or derived from recordings (Abrahamson and Silva 1997, Campbell 1997). For a censored Poisson process, MAR or Annual Probability are related through Eq. (1).

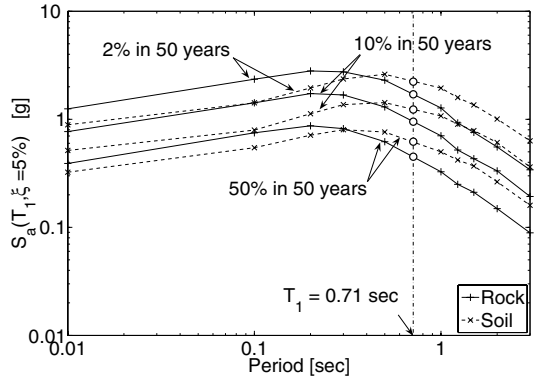

Figure 21. Uniform hazard spectra for HBMC Bridge site

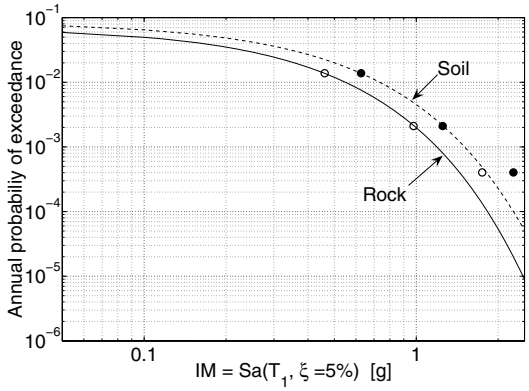

Figure 22. Seismic hazard curves of HBMC Bridge site

Uniform hazard spectra for the site (see Fig. 21) were obtained from the USGS probabilistic seismic hazard maps for rock site condition (NEHRP site category B/C). These spectra were then modified to include near-fault rupture directivity effects. Soil site spectra were generated from the rock site spectra by using empirical soil-to-rock spectrum ratio (Abrahamson and Silva 1997). Three seismic hazard levels were selected, defined by 50%, 10%, and 2% probability of exceedance in 50 years (with a return period of 73, 475 and 2475 years, respectively). These seismic hazard levels are also referred to in the literature (e.g., seismic codes) as the Serviceability Earthquake (or Moderate Event), Design Earthquake (or Design Event), and Maximum Earthquake (or Maximum Credible Earthquake), respectively (ATC-40 1996). The *seismic hazard curves* (in terms of annual probability of exceedance) for soil and rock site conditions are approximated by fitting a Gumbel probability distribution to the spectral acceleration $S_a(T_1 = 0.71\text{sec}, \xi = 5\%)$ at the three seismic hazard levels defined above, see Fig. 22 (Zhang et al. 2007). The seismic hazard curves account for the randomness/uncertainty in (1) the temporal and spa-

tial occurrences of earthquakes, (2) the magnitude and source-to-site distance, and (3) the attenuation of the ground motion intensity with magnitude and distance.

Ensembles of Ground Motion Time Histories. A total of 51 ground motion time histories were selected by Somerville and Collins (2002) to satisfy to the extent possible (1) the dominant magnitude and distance combinations indicated by the M-R deaggregation of the seismic hazard at the three hazard levels considered, and (2) the local geological and seismological conditions (e.g., fault mechanism, near fault effects). At the "50% in 50 years" hazard level, the 22 recordings (17 soil records and 5 rock records) are from earthquakes in the Cape Mendocino, California region. At the "10% in 50 years" hazard level, the recordings (15 soil records and 4 rock records) are from diverse earthquakes: two from the 1992 Cape Mendocino earthquake, two from the 1978 Tabas, Iran earthquake, and the remaining fifteen from the 1999 Chi-Chi, Taiwan earthquake. At the "2% in 50 years" hazard level, the 10 recordings (2 soil records and 8 rock records) come from large interplate subduction earthquakes: the 1985 Valparaiso, Chile, and Michoacan, Mexico earthquakes. Each selected ground motion time history is scaled such that the corresponding spectral acceleration at T_1 = 0.71sec matches the uniform hazard spectrum at the appropriate hazard level (see Fig. 23).

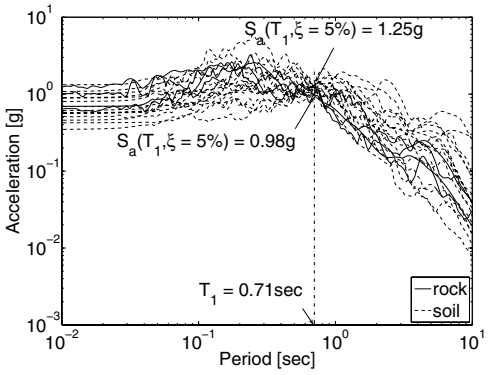

Figure 23. Spectral acceleration of scaled ground motions at the 10% in 50 years hazard level

5 PROBABILISTIC SEISMIC DEMAND HAZARD ANALYSIS (PSDHA)

The next step is to estimate in probabilistic terms the seismic demand that future possible earthquake ground motions will impose on the structure. The objective of PSDHA is to compute the MAR, $\lambda_{EDP}(\delta)$, of a given structural response parameter, called Engineering Demand Parameter (*EDP*) in the PEER PBEE framework, exceeding a specified threshold value δ. The *EDP*s considered in this study to capture three critical potential failure modes were defined in Section 3. *EDP*s depend on both seismic excitation and system properties **Y** (e.g., geometric, material, inertia, and damping properties). Past research has shown that a judiciously defined *IM* (such as spectral acceleration at the fundamental period of the structure) renders any *EDP* approximately conditionally independent, given *IM*, of earthquake magnitude (*M*), source-to-site distance (*R*) and any other ground motion characteristics (Shome et al. 1998, Luco and Cornell 2006). Thus, any *EDP* can be expressed as

$$EDP(\mathbf{Y}, M, R, IM, ..., \varepsilon_I, \varepsilon_E) \approx EDP(\mathbf{Y}, IM, \varepsilon_I, \varepsilon_E) \quad (3)$$

where ε_I = random variable representing the effect of record-to-record variability on the *EDP*, ε_E = random variable representing the effects of epistemic uncertainties (e.g., FE modeling uncertainty and statistical parameter uncertainty) in determining the *EDP* for a given ground motion input and given system properties. The epistemic uncertainties in *EDP*s are not considered in this study. First, the system properties are assumed deterministic, i.e., a deterministic estimate of **Y**, $\bar{\mathbf{y}}$, was taken as the nominal (best estimate) values of the system properties. The probability, $P\left[EDP(\bar{\mathbf{y}}, IM, \varepsilon_I) > \delta\right]$, can be obtained using the TPT as

$$P\left[EDP(\bar{\mathbf{y}}, IM, \varepsilon_I) > \delta\right] = \int_{IM} P\left[EDP(\bar{\mathbf{y}}, IM, \varepsilon_I) > \delta \middle| IM = im\right] f_{IM}(im)\, dim \quad (4)$$

where $f_{IM}(im)$ is the PDF of *IM* for a random earthquake and is related to the seismic hazard curve, $\nu_{IM}(im)$, as

$$\left|\frac{d\nu_{IM}(im)}{dim}\right| = \left|\frac{d\left(\nu P[IM > im]\right)}{dim}\right| = \nu f_{IM}(im) \quad (5)$$

Substituting Eq. (5) into Eq. (4) yields the following MAR of occurrence of random demand events $\{EDP(\bar{\mathbf{y}}, IM, \varepsilon_I) > \delta\}$:

$$\nu_{EDP}(\delta) = \nu P\left[EDP(\bar{\mathbf{y}}, IM, \varepsilon_I) > \delta\right] = \int_{IM} P\left[EDP(\bar{\mathbf{y}}, IM, \varepsilon_I) > \delta \middle| IM = im\right] \left|d\nu_{IM}(im)\right| \quad (6)$$

Thus the *demand hazard curve* $\nu_{EDP}(\delta)$ is obtained mathematically as the convolution of the conditional complementary CDF of the *EDP* given *IM* with the seismic hazard curve $\nu_{IM}(im)$. In Eq. (6), the probability distribution $P\left[EDP(\bar{\mathbf{y}}, IM, \varepsilon_I) > \delta \middle| IM = im\right]$ expresses the effects of record-to-record random variability, ε_I, on the *EDP* given *IM*. The FE model of the BFG system (Fig. 2) is subjected to the ensembles of scaled ground motion records (defined in Section 4) to estimate the conditional probability distributions, given *IM*, of the *EDP*s selected at each of the three *IM* levels considered. Then, these estimated probability distributions at discrete *IM* levels

are interpolated/extrapolated over the continuum range of *IM* values contributing appreciably to the MAR of limit-state exceedance. The bridge responses to the seismic inputs derived from the soil free-field motions and rock free-field motions are treated separately. As an illustration, Fig. 24 shows, together with the seismic hazard curves ($\nu_{IM}(im)$) for both rock and soil free-field input motions, the FE based simulation results (solid dots) and their fitted probability distributions, given *IM*, for the maximum (over all piers) peak lateral drift, Δ^P, at the three hazard levels considered and for the rock and soil free-field input motions treated separately. Based on empirical determination of their probability distribution models, the *EDP*s Δ^P, Δ_{abut}^{UNS} and Δ_{exp}^{UNS} given *IM* are assumed to follow the lognormal distribution, i.e.,

$$P\left[EDP \le \delta \middle| IM = im\right] = \Phi\left(\frac{\ln\delta - \lambda(im)}{\zeta(im)}\right), \quad \delta > 0 \qquad (7)$$

where $\lambda(im)$ and $\zeta(im)$ denote the mean and standard deviation of the natural logarithm of the *EDP*, respectively. The conditional probability distributions of the other *EDP*s (Δ_{abut}^{SK}, Δ_{exp}^{SK} and Δ_{cont}^{SK}) given *IM* are assumed to follow the hybrid lognormal distribution, truncated at the shear keys' ultimate deformation capacity $\Delta_u^{sk} = 100mm$(4in) (Zhang et al. 2007b). The distribution parameters, e.g., λ and ζ, are determined through least squares fitting of the assumed probability distribution, e.g., Eq. (7), to the simulated *EDP*s using the FE model of the BFG system at the three discrete hazard levels. The distribution parameters are then approximated as continuous functions of *im, e.g.,* $\lambda(im)$ and $\zeta(im)$ (Zhang et al. 2007b). In the case of a lognormal *EDP*, $\exp\left[\lambda(im)\right]$ corresponds to the median of the *EDP*, while $\exp\left[\lambda(im)-\zeta(im)\right]$ and $\exp\left[\lambda(im)+\zeta(im)\right]$ correspond to the 16- and 84-percentile of the *EDP*, respectively. Approximations of the median value and 16/84-percentile of Δ^P as functions of *im* are also plotted in Fig. 24.

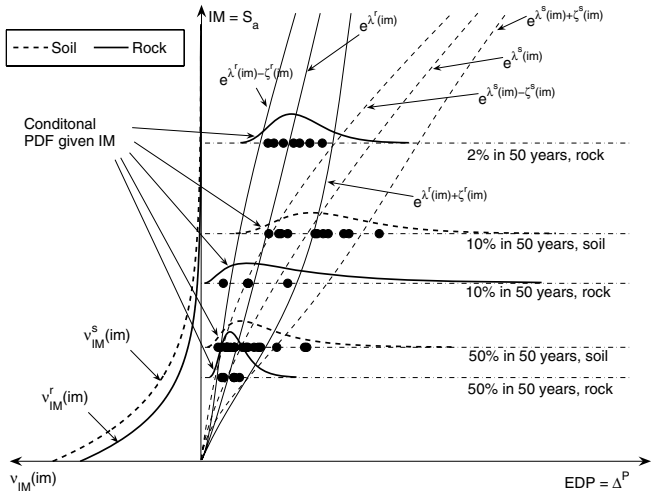

Figure 24. Probabilistic response analysis conditional on *IM* and "no collapse"

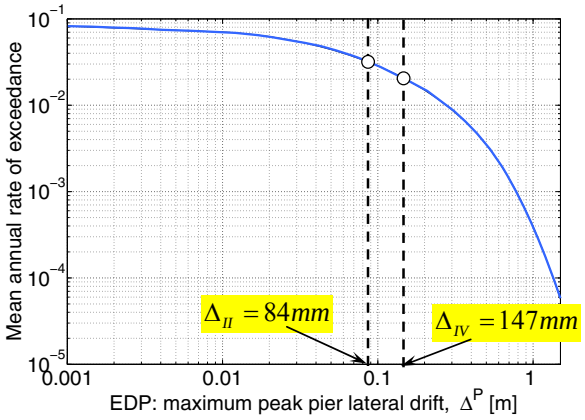

Figure 25. Seismic demand hazard curve for Δ^P

The nonlinear response history analyses performed indicate that the bridge collapses (global dynamic instability) in 3 out of 15 "10% in 50 years" soil free-field ground motions and 1 out of 8 "2% in 50 years" rock free-field ground motions. Thus, Eq. (6) needs to be modified to incorporate the possibility of collapse. Let *C* denote the collapse event and $P\left[C \middle| IM = im\right]$ denote the conditional probability of collapse given *IM*. This conditional probability is estimated, similarly to $P\left[EDP > \delta \middle| IM = im\right]$, through the ensembles of nonlinear time history analyses with rock and soil free-field input motions treated separately. It can then be shown that the MAR of occurrence of events $\{EDP > \delta\}$ becomes

$$\nu_{EDP}(\delta) = \int_{IM} P\left[C \middle| IM\right] \left|d\nu_{IM}\right| + \int_{IM} P\left[EDP > \delta \middle| IM, C^c\right] P\left[C^c \middle| IM\right] \left|d\nu_{IM}\right| \qquad (8)$$

Using Eq. (8), seismic demand hazard curves are derived separately for the two sets of rock and soil free-field input motions. A combined seismic demand hazard curve is then obtained as the following "weighted average" of the demand hazard curves for the two sets of free-field input motions (Zhang et al. 2007b):

$$\nu_{EDP}(\delta) = \int_{IM} P\left[EDP > \delta \middle| IM, Rock\right] \frac{n_r(im)}{n_r(im) + n_s(im)} \left|d\nu_{IM,Rock}\right| + \int_{IM} P\left[EDP > \delta \middle| IM, Soil\right] \frac{n_s(im)}{n_r(im) + n_s(im)} \left|d\nu_{IM,Soil}\right| \qquad (9)$$

where $n_r(im)$ and $n_s(im)$ denote the number of rock and soil free-field input motions, respectively, at hazard level *im*. As an illustration, the seismic demand hazard curve for Δ^P obtained from Eq. (9) is shown in Fig. 25. Similarly, seismic demand hazard curves were obtained for the other system-level *EDP*s defined in Section 3 (Zhang et al. 2007b).

In the PBEE framework described above, the variables *IM* and *EDP* (for a single limit-state) can be vector-valued, in which case the integrals over *IM* and *EDP* in the above equations become multifold.

6 PROBABILISTIC CAPACITY ANALYSIS (FRAGILITY ANALYSIS)

The objective of this third analytical step of the PEER PBEE methodology is to compute the mean rate of exceedance of a specified limit-state given the *EDP*s associated to this limit-state. Typically, limit-state functions are expressed as

$$\begin{aligned} g &= R - S = \hat{R}(\bar{\mathbf{y}}) + \varepsilon_R - EDP + \varepsilon_G \\ &= g(\bar{\mathbf{y}}, IM, \varepsilon_I, \varepsilon_R, \varepsilon_G) \end{aligned} \tag{10}$$

where $\hat{R}(\bar{\mathbf{y}})$ is the deterministic capacity predicted based on the nominal values of the system properties $\bar{\mathbf{y}}$; and ε_R and ε_G are random variables representing the uncertain level of inaccuracy of the capacity model used (e.g., discrepancy between deterministic predictions based on nominal geometric and material parameter values and experimental measurements of the capacity) and the inexactness of the limit-state function (due to missing demand variables affecting the considered limit-state), respectively. In this study, it is assumed that a single (scalar) *EDP* is associated with each limit-state of each failure mechanism.

It can be shown that the mean rate of occurrence of random events $\{g(\bar{\mathbf{y}}, IM, \varepsilon_I, \varepsilon) < 0\}$, accounting for the uncertainty in the inexactness of the capacity model and limit-state function as represented by random variable $\varepsilon = \varepsilon_R + \varepsilon_G$, is given by (Zhang el al. 2007b)

$$\begin{aligned} &\nu\{g(\bar{\mathbf{y}}, IM, \varepsilon_I, \varepsilon) < 0\} = \\ &\int_{EDP} P[g(\bar{\mathbf{y}}, \varepsilon) < 0 | EDP = \delta] \cdot |d\nu_{EDP}(\delta)| \end{aligned} \tag{11}$$

The conditional probability of exceeding the limit-state function (i.e., $g(\bar{\mathbf{y}}, \varepsilon) < 0$) given $EDP = \delta$, $P[g(\bar{\mathbf{y}}, \varepsilon) < 0 | EDP = \delta]$, accounts for the uncertainties in the predictive (nominal) capacity model and limit-state function and is referred to as *fragility function/curve* in the literature. Thus, according to the above equation, the mean rate of exceedance of a specified limit-state is obtained mathematically as the convolution of the fragility curve and the seismic demand hazard curve, ν_{EDP}, of the *EDP* used in defining the limit-state function.

The univariate probabilistic capacity models (or fragility curves) developed in this study to assess the fragility of the HBMC Bridge in regards to its most critical potential failure mechanisms are based on existing and newly developed deterministic predictive capacity models and experimental data. For each limit-state considered, a set of experimental data was collected from previous tests. For each experimental specimen considered, the measured-to-predicted capacity ratio is computed. If the predictive capacity model were perfect and in the absence of inherent and modeling uncertainties and measurement noise/errors, these measured-to-predicted capacity ratios would all be unity and, therefore, the fragility function would take the form of a step function centered at the unit value. However, in reality, these ratios exhibit a scatter due to imperfect capacity models, missing explanatory variables, and various sources of randomness/uncertainty. In this study, these ratios are approximated by the Normal distribution for each limit-state of each failure mechanism. Thus, the fragility curves are obtained by least-square fitting the Normal CDF to the empirical CDF defined by these computed measured-to-predicted ratios for each limit-state. The uncertainty of the capacity ratio decreases with increase of the slope of the fragility curve, while the bias of the predictive capacity model is given by the ratio corresponding to a fragility value of 50%. If the bias is unity, then the predictive capacity model is unbiased.

A refined deterministic, mechanistic model (Acero et al. 2006) was developed to predict the capacity of a lap-spliced pier against each of the five limit-states of pier flexural failure in the lap-spliced region. This capacity model accounts for (1) the force transfer mechanism between spliced rebars, (2) the bond-slip degradation, (3) the length of the yield plateau in the stress-strain law of the spliced reinforcing steel, (4) the length of the spliced region, (5) the strain penetration of the longitudinal reinforcement into the foundation (pile cap), and (6) the axial load ratio. This capacity model was calibrated using experimental data on lap-spliced columns. The deformation-based (in terms of pier lateral drift) predicted capacities have the advantage of being rather insensitive to the change in the axial load ratio ranging from 0.9% to 7.1% during the earthquake response simulations performed. Therefore, in this study, the predictive capacity (denominator of the measured-to-capacity ratio) for each limit-state is computed for the axial load ratio under gravity loads alone. The experimental data used to develop the fragility curves for flexural failure of lap-spliced piers originate from 10 lap-spliced column specimens, four of them tested at UCSD (Hose and Seible 1999) and the remaining six tested at UCLA (Melek et al. 2003). Each test specimen provides two data points (in the push and pull direction, respectively) for each limit-state. As illustration, Fig. 26 shows

the fragility curve for joint limit-state III-IV-V of the pier flexural failure mechanism together with the 20 values of the measure-to-predicted capacity ratio used to fit the fragility curve. The deformation capacities of a typical pier (average height of 12*m*) of the HBMC Bridge for LS-II and LS-III-IV-V predicted using the above-referred mechanistic model and the nominal geometric and material parameter values given in (Zhang et al. 2006a) are 84*mm* and 147*mm*, respectively.

For the shear key(s) failure mechanism, a predictive capacity model based on the strut-and-tie approach (Megally et al. 2001) was adopted. Experimental tests for (unconfined) shear keys are scarce, and the fragility curves for the shear key(s) failure mechanism were based on the results of the following experimental tests: 3 tests by (Megally et al. 2001) and 2 tests by (Bozorgzadeh et al. 2004). As illustration, Fig. 27 shows the fragility curve and corresponding measured-to-predicted capacity ratios for limit-state IV of shear key failure.

For unseating of the superstructure, the predicted deformation capacity is taken here as the width of the seat (737mm/29in) at the abutments or half the pier width (610mm/24in) at the interior expansion joints. Unfortunately, no experimental or field data could be found for the unseating failure mechanism and the fragility curve shown in Fig. 28 was defined based on engineering judgment.

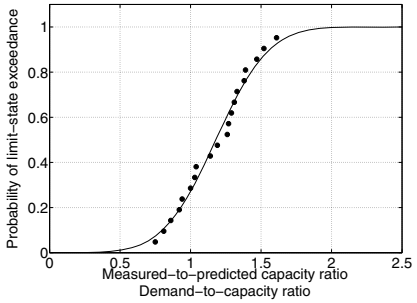

Figure 26. Fragility curve for joint limit-state III-IV-V of pier flexural failure ($EDP = \Delta^{P}$)

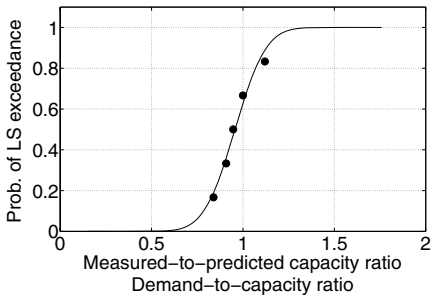

Figure 27. Fragility curve for limit-state IV of shear key failure ($EDP = \Delta^{SK}_{abut}$, Δ^{SK}_{exp}, Δ^{SK}_{cont})

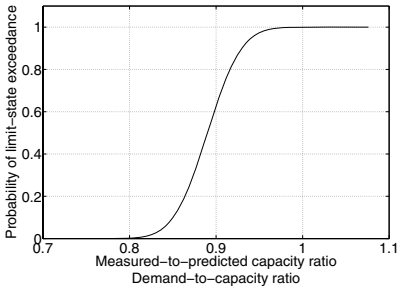

Figure 28. Fragility curve for limit-state V of unseating failure mechanism ($EDP = \Delta^{UNS}_{abut}$, $\Delta^{UNS}_{\exp}$)

7 SEISMIC RELIABILITY ANALYSIS

For each of the three failure mechanisms and corresponding limit-states considered, the MAR of limit-state exceedance is obtained by convolving the appropriate fragility curve, $P\left[g(\bar{\mathbf{y}},\varepsilon)<0 \middle| EDP=\delta\right]$, with the demand hazard curve of the associated *EDP*, $\nu_{EDP}(\delta)$, as expressed by Eq. (11). The computed MARs of limit-state exceedance and corresponding return periods (defined as the reciprocal of the MARs of exceedance) are reported in Table 1 for all limit-states considered in this study.

The seismic reliability assessment results obtained in this study reveal that, among the potential limit-states considered, the most critical ones are the initiation (return period from 12 to 22 years) and full development (return period from 14 to 26 years) of the shear key failure mechanism, especially at the abutments and interior expansion joints. However, the return period of the strength degradation limit-state (LS-V) of the shear key failure mechanism is significantly longer (100 years at the abutment shear keys and 172 years at the expansion joint shear keys) than the return period for the lower limit-states I-II-III and IV. It is found that the strength degradation limit-state of the shear keys at the continuous joints is virtually impossible (computed return period of 12,500 years). The lap-spliced pier flexural failure mechanism is also critical with a return period of 29 years for the yielding limit-state and 48 years for the strength degradation limit-state. Thus, the pier flexural failure mechanism is the most critical one causing an overall collapse of the bridge. It is also observed from the results in Table 1 that unseating is a very unlikely failure mechanism of the bridge. This is most likely due to the typical deformation pattern (see Fig. 17) of the BFG system when subjected to strong seismic excitation. Due to soil lateral spreading, the superstructure of the bridge, including the abutments, is in an overall compressive mode, thus increasing the safety of the bridge against unseating.

Overall, the seismic reliability analysis results given in Table 1 justify the retrofit efforts (see Section 1) performed by Caltrans on the HBMC Bridge.

Table 1. Computed Mean annual rate of exceedance (Return Period) of limit-states considered

Failure Mechanism	**Limit-State**	**MAR of Exceedance**	**Return Period** (Years)
Flexural failure at lap-spliced piers	II: Yielding of reinforcement	0.034	29.4
	III-IV-V: Initiation of failure mechanism; full formation of failure mechanism; strength degradation	0.021	47.6
Failure of shear keys at abutments	I-II-III: Onset of cracking; yielding of reinforcement; large open cracks and onset of concrete spalling	0.080	12.5
	IV: Cracks and spalling over the full region of the shear key	0.069	14.5
	V: Loss of load-carrying capacity; fracture of reinforcement	0.010	100
Failure of shear keys at continuous joints	I-II-III: same as above	0.046	22
	IV: same as above	0.039	26
	V: same as above	8.0×10^{-5}	12,500
Failure of shear keys at interior expansion joints	I-II-III: same as above	0.064	15.6
	IV: same as above	0.058	17.2
	V: same as above	0.0058	172.4
Unseating at abutments	V: Collapse	0.0011	909
Unseating at interior expansion joints	V: Collapse	0.0012	833

8 PROBABILISTIC LOSS ANALYSIS

In the PEER PBEE methodology, the probabilistic performance assessment results presented in the previous section can be propagated further to decision variables (*DV*s) that relate to casualties, cost, and downtime and are of great interest to stakeholders. The objective of probabilistic seismic loss analysis is to assess *DV*s probabilistically (e.g., compute the MAR of the total repair/replacement cost due to seismic damage exceeding a specified dollar amount) for a given structure at a given location. This study considers a single *DV*, namely the total repair/replacement cost to restore the bridge to its pre-earthquake state. The probabilistic assessment of this *DV*, which is a random variable, accounts for the uncertainties in the seismic hazard at the site or in *IM* (see Section 4), in the seismic demand (*EDP*s) (see Section 5), in the structural capacity and damage/limit-states (see Section 6), and in the cost associated with the repair of individual structural components or replacement of the entire bridge. This study does not account for the uncertainty/randomness in system properties. The outcome of the present probabilistic loss analysis is *the seismic loss hazard curve*, which expresses the MAR of the total repair/replacement cost exceeding any specified threshold value.

In the case of global failure of the bridge, a new bridge will be constructed and the total repair cost is defined by the construction cost of the new bridge. In the case of "no global collapse", it is assumed that all damage occurs at the component level and the total repair cost (L_T) of the bridge (in a year) is equal to the summation of the repair costs of all components damaged during this year, i.e.,

$$L_T = \sum_{j=1}^{n} L_j \tag{12}$$

where L_j is the repair cost of the j^{th} damaged component, and n is the number of damaged components (i.e., piers, shear keys, spans) in the bridge. The repair cost of a damaged component is generally associated with a specified repair scheme, which is again associated with the damage state of the component.

To overcome a number of difficulties associated with a multi-hazard integral approach (Conte et al. 2007), a very efficient multilayer Monte Carlo simulation (MCS) approach is used in this study to estimate the seismic loss hazard curve related to L_T. MCS can incorporate and propagate the uncertainties in all random variables involved in the seismic loss analysis, namely *IM*, *EDP*s, *DM*s and *DV*s. The acronym *DM*s stands for Damage Measures, which are equivalent to limit-states (I, II, III, IV, V) defined earlier (see Section 3). A large number of MC samples are required to obtain a sufficiently accurate probabilistic estimate of the seismic loss hazard curve. Fig. 29 presents an overview of the multilayer Monte Carlo simulation approach used in this study. The number of earthquakes in each year is simulated according to the Poisson random occurrence model in Eq. (1). For each earthquake, an *IM* value is generated randomly according to its PDF derived from the seismic hazard curve. For this *IM* value, the event of collapse or no collapse is simu-

lated randomly according to the conditional probability $P[C \mid IM = im]$ (see Section 5). In the case of collapse, L_T is randomly generated from the probability distribution of the rebuilding cost and this single earthquake simulation is ended. In the case of no collapse, a set of *EDP*s ($\Delta^P, \Delta^{SK}_{abut}, \Delta^{SK}_{exp}, \Delta^{SK}_{cont}, \Delta^{UNS}_{abut}, \Delta^{UNS}_{exp}$) must be randomly generated. The needed conditional joint PDF of the *EDP*s given *IM* is constructed using the NATAF model (Nataf 1962) and the marginal probability distributions and correlation coefficients of the *EDP*s estimated from the results of the ensemble FE response simulations performed at the three hazard levels and interpolated/extrapolated over the continuum range of *IM* values. As shown in Fig. 30, each and every of these *EDP* values is entered into its corresponding fragility curve to determine the probability of each damage state of the appropriate component as

$$P[DM = k \mid EDP = \delta] = P[g_k < 0 \mid EDP = \delta] - P[g_{k+1} < 0 \mid EDP = \delta] \quad (13)$$

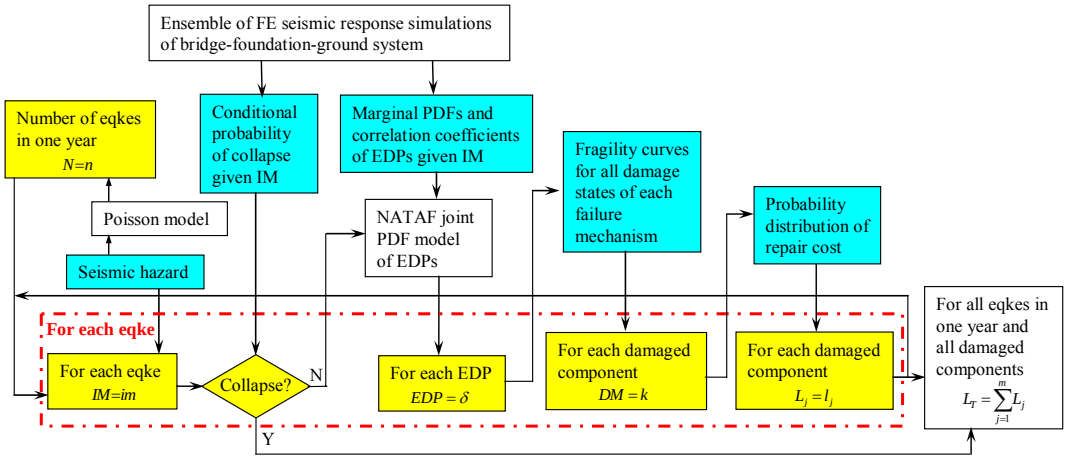

Fig. 29: Multilayer Monte Carlo simulation approach for probabilistic seismic loss estimation

For each damage component, a damage state is randomly generated according to the probability mass function defined in Eq. (13) and then a repair cost is generated according to its probability distribution. The total repair cost L_j for this single earthquake simulation is equal to the sum of all the simulated component repair costs. This single year and single earthquake simulation is repeated a large number of times (e.g., 10,000 years with one or more earthquakes) to estimate the conditional complementary CDF of the total annual repair cost, $P[L_T > l \mid IM > 0]$, given the occurrence of one or more earthquake(s) in the considered year. Using the TPT, the probability of the total annual repair/replacement cost exceeding a specified threshold value, $l > 0$, is obtained as

$$P[L_T > l] = P[L_T > l \mid IM = 0]P[IM = 0] + P[L_T > l \mid IM > 0]P[IM > 0] \quad (14)$$

Since the total annual repair/replacement cost is zero if no earthquake occurs during this year, Eq. (14) reduces to

$$P[L_T > l] = P[L_T > l \mid IM > 0]P[IM > 0] \quad (15)$$

The conditional probability on the RHS of Eq. (15) is estimated using the multilayer Monte Carlo simulation approach described above. Using the censored Poisson assumption, the probability $P[IM > 0]$ can be obtained from the seismic hazard curve as

$$P[IM > 0] = 1 - \exp[-\nu_{IM}(0)] \quad (16)$$

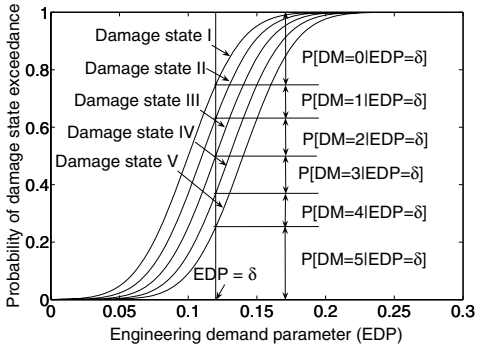

Fig. 30: Conditional probability of damage state given the *EDP*

Basic ingredients to probabilistic loss assessment are repair actions and probability distributions of their costs given the component damage states (see Fig. 31). In this study, this information was obtained, with the help of engineers from LAN Engineering in Irvine, California, from the two Caltrans retrofits on the HBMC Bridge (see Section 1) and similar work done on highway bridges in different districts throughout California. The repair costs were calculated based on the recent empirical unit cost data (Caltrans 2003) and the quantities of repair work required form the HBMC Bridge. The mean and coefficient-of-variation (ratio of standard deviation over the mean) of component repair costs given the damage state are given in Table 2. The zero repair cost

for damage state II of pier flexural failure indicates that no repair is required in practice for this damage level. The repair costs for damage states IV and V of shear key failure are identical because the same repair actions are required. The conditional probability distributions of component repair cost given the damage state are all assumed normally distributed.

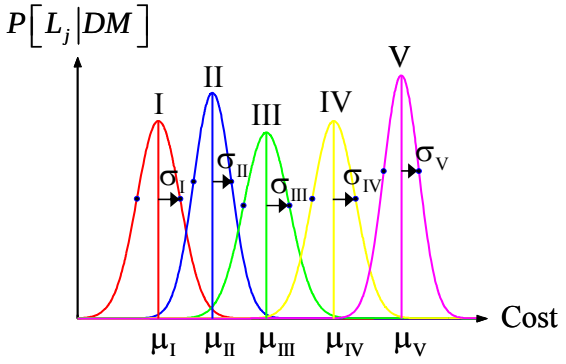

Fig. 31: Conditional probability distributions of component repair cost given the damage state

Table 2. Statistics of component repair costs as a function of damage state

Failure Mechanism	Damage State	Unit Repair Cost	
		Mean	c.o.v.
Flexural failure at lap spliced piers	II: Yielding	0	--
	IV: Full development of mechanism	$246,500	0.10
Failure of shear keys at abutments	III: Initiation of mechanism	$10,400	0.10
	IV: Full development of mechanism	$137,600	0.16
	V: Strength degradation	$137.600	0.16
Failure of shear keys at continuous joints	III: Initiation of mechanism	$10,400	0.10
	IV: Full development of mechanism	$137,600	0.16
	V: Strength degradation	$137.600	0.16
Failure of shear keys at interior expansion joints	III: Initiation of mechanism	$10,400	0.10
	IV: Full development of mechanism	$137,600	0.16
	V: Strength degradation	$137.600	0.16
Unseating at abutments	V: Collapse	$22,300	0.18
Unseating at interior expansion joints	V: Collapse	$22,300	0.18
Collapse	N/A	$24,000,000	0.12

The seismic loss hazard curves were computed using Eq. (15) for rock and soil free-field input motions considered separately. The solid curve in Fig. 32 is the average of the loss hazard curves for rock and soil free-field input motions. According to this loss hazard curve, the total annual repair/replacement cost is very unlikely to exceed $3.6M dollars as the corresponding return period is about 1,000 years.

A number of very useful information can be obtained from the results of probabilistic seismic loss analysis using the multilayer Monte Carlo simulation approach presented above. For example, Fig. 33 shows the contributions to the expected (mean) total repair/replacement cost per earthquake at a specified

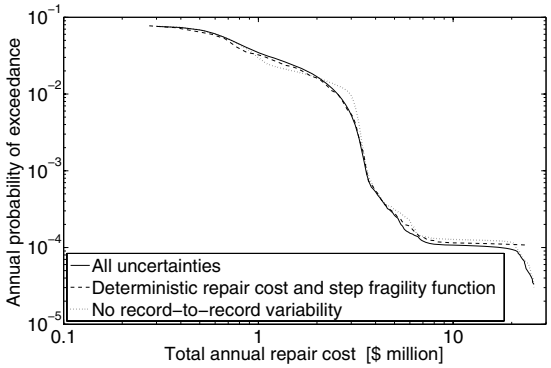

Fig. 32: Annual probability of total seismic repair/replacement cost exceeding a specified threshold value

IM of the various groups of damaged components (piers, shear keys, spans). It is observed that at low *IM* level (< 0.2g), the total repair/replacement cost is mostly contributed by shear key failures. For *IM* between 0.2g and 1.5g, the total repair/replacement cost is predominantly contributed by the shear key

failures and pier flexural failures. For *IM* above 1.5g, the loss due to overall collapse of the bridge becomes increasingly dominant, and the steep slope of the curve representing the expected total repair/replacement cost for *IM* between 2g and 3g is due to the fast increase of the conditional probability of collapse $P[C \mid IM]$ in this range. The expected total repair cost per earthquake converges asymptotically to the expected (mean) rebuilding cost ($24M dollars) as *IM* increases. It is noticed that the unseating failure mechanism hardly makes any contribution to the expected total repair/replacement cost per earthquake, because of its very low probability of occurrence (see Table 1) and its relatively low repair cost (see Table 2).

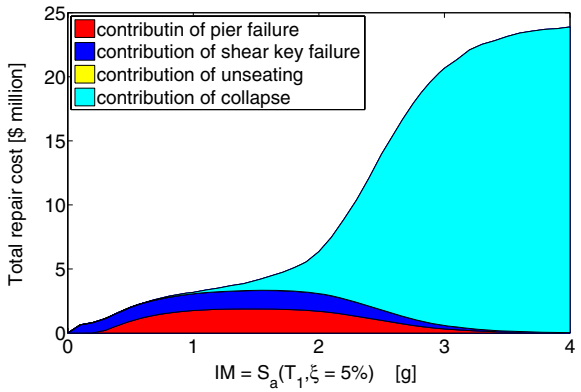

Fig. 33: Contributions of different failure mechanisms to the expected total repair/replacement cost per earthquake at specified IM level

The loss hazard curve in solid line in Fig. 32 incorporates the effects of the uncertainties related to earthquake occurrences in space and time, ground motion intensity, ground motion time history (record-to-record variability), structural capacity, damage/limit-states, and repair costs. It is of interest to investigate the relative importance of these various sources of uncertainty in regards to the loss hazard results. For this purpose, additional parametric studies were conducted. For example, the loss hazard curve in dashed line in Fig. 32 was obtained by neglecting the uncertainties related to structural capacity and damage states (i.e., representing each fragility curve by a step function with the step located at the predicted/nominal capacity) and the repair costs at various damage states (i.e., treating repair costs deterministically at their mean values). As can be seen, the combined effect of these two sources of uncertainty is small. In another "what if" study, only the effect of record-to-record variability was removed in the loss analysis (i.e., each *EDP* at any *IM* level was treated as deterministic equal to its mean value). The corresponding loss hazard curve is the dotted one shown in Fig. 32. It is observed that the record-to-record variability (i.e., randomness in ground motion time history) has appreciable effects on the loss hazard curve. These parametric studies indicate that the uncertainty related to *IM* (emanating from the uncertainties in earthquake occurrence in space and time, earthquake magnitude, site-to-source distance, wave propagation path, attenuation relations) and represented in the form of a seismic hazard curve, is the dominant source of uncertainty in probabilistic seismic loss analysis of the HBMC bridge testbed.

9 CONCLUSIONS

This paper presents the analysis of the Humboldt Bay Middle Channel (HBMC) Bridge testbed near Eureka in northern California using the performance-based earthquake engineering (PBEE) methodology developed at the Pacific Earthquake Engineering Research (PEER) Center. This probabilistic performance assessment methodology integrates four analytical steps, namely (1) probabilistic seismic hazard analysis in terms of a ground motion intensity measure (*IM*), (2) probabilistic seismic demand analysis given *IM*, in terms of engineering demand parameters (*EDP*s), (3) probabilistic capacity analysis (or fragility analysis) for various limit-states associated with the critical potential failure modes of the system, and (4) probabilistic loss analysis. The seismic demand analysis was performed based on a two-dimensional nonlinear finite element model of the bridge-foundation-ground (BFG) system developed in the software framework OpenSees. Under strong earthquakes, the response of the bridge is controlled by soil lateral spreading mechanisms associated with soil liquefaction. In this study, *IM* was taken as the 5% damped elastic spectral acceleration at the first (low amplitude vibration) period of the computational model of the BFG system.

The basic sources of uncertainty represented in the PEER PBEE methodology are related to: occurrence of earthquakes in space and time, earthquake magnitude, wave propagation path/attenuation, ground motion intensity, ground motion time history (i.e., record-to-record variability), structural capacity, damage/limit-states, and repair costs. Uncertainty in material and system parameters (i.e., FE model parameters) are not considered in this paper.

The outcome of analytical step (1) is a seismic hazard curve for the site of the bridge, which expresses the mean annual rate (MAR) of *IM* exceeding any specified threshold value. The integration of analytical steps (1) and (2) provides a seismic demand hazard curve for each *EDP*, which represents the MAR of this *EDP* exceeding any specified threshold value.

Three potential failure mechanisms were considered, namely flexural failure of lap-spliced piers, failure of shear keys, and unseating. For each failure mechanism, five limit-states were defined, each associated with a single *EDP*. The outcome of analyti-

cal step (3) is a fragility function/curve for every limit-state of every failure mechanism considered. Such a fragility curve provides the conditional probability of limit-state exceedance given the associated *EDP*. Fragility curves are developed based on predictive modeling and experimental data.

The MAR of limit-state exceedance is obtained by convolving the corresponding fragility curve with the demand hazard curve for the *EDP* associated to this limit-state.

In this study, probabilistic seismic loss analysis – analytical step (4) – was performed using a multi-layer Monte Carlo simulation approach. The outcome is a seismic loss hazard curve, which expresses the MAR of a decision variable (typically related to casualties, cost, and downtime) exceeding a threshold value. The single decision variable considered in this study was the total annual repair/replacement cost of the bridge due to earthquakes.

Investigation of the relative importance of the various sources of uncertainty on the seismic loss results revealed that the uncertainty related to *IM* (as represented by the seismic hazard curve) is the dominant source of uncertainty and that record-to-record variability has an appreciable effect on the loss hazard curve. The other sources of uncertainty were found to have only minor effects on the loss hazard curve.

In future research, it will be important to evaluate the robustness of the probabilistic performance assessment results to the various assumptions and simplifications made in applying the PEER PBEE methodology.

ACKNOWLEDGEMENTS

This work was supported by the Earthquake Engineering Research Centers Program of the National Science Foundation, under Award Number EEC-9701568 through the Pacific Earthquake Engineering Research Center (PEER). Any opinions, findings and conclusions or recommendations expressed in this material are those of the authors and do not necessarily reflect those of the National Science Foundation. This support is gratefully acknowledged. The authors wish to thank Mr. Patrick Hipley, Dr. Cliff Roblee, Dr. Charles Sikorsky, Mr. Mark Yashinsky, and Mr. Tom Shantz of Caltrans for providing all the requested information regarding the initial design and retrofits of the Humboldt Bay Middle Channel Bridge. Dr. Zhaohui Yang, Prof. Ahmed Elgamal and Prof. Jose Restrepo at U.C. San Diego, Prof. Greg Fenves and Dr. Frank McKenna at U.C. Berkeley, Prof. Michael Scott (Oregon State University), and Prof. Jacobo Bielak (Carnegie Mellon University) helped with the geotechnical and structural modeling and analysis aspects of this work. Their help is gratefully acknowledged. The authors also want to thank Dr. Paul Somerville (URS Corporation), Prof. C. Allin Cornell (Stanford Univ.), Prof. Armen Der Kiureghian (U.C. Berkeley) and Prof. Mark Eberhard (Univ. of Washington) for insightful discussions on probabilistic seismic hazard analysis, probabilistic performance assessment, and fragility analysis. Mr. Gabriel Acero who performed the work on fragility analysis as part of his M.S. thesis at U.C. San Diego is also gratefully acknowledged.

BIBLIOGRAPHY

Abrahamson, N.A., Silva, W.J., 1997. Empirical response spectral attenuation relations for shallow crustal earthquakes. *Seismological Research Letter*, 68(1), 94-109.

Acero, G., Restrepo, J.I., Conte, J.P., Zhang, Y., 2006. Seismic response of columns with unconfined lap-splices. In preparation for submission to *ACI Structural Journal*.

Ang, A.H., Tang, W.H., 2007. *Probability Concepts in Engineering: Emphasis on Applications to Civil and Environmental Engineering*. Second Edition, Wiley.

Benjamin, J., Cornell, C.A., 1970. *Probability, statistics and decision for civil engineers*. McGraw-Hill, New York.

Caltrans. 2003. Contract cost data, a summary of cost by items for highway construction projects. *Business, Transportation, and Housing Agency*, Department of Transportation, State of California.

Campbell, K.W., 1997. Attenuation relationships for shallow crustal earthquakes based on California strong motion data. *Seismological Research Letter*, 68(1), 180-189.

Conte, J.P., Zhang, Y., Acero, G., Char, M., 2007. Probabilistic seismic loss assessment of Humboldt Bay Middle Channel Bridge. In preparation for submission to *Earthquake Engineering and Structural Dynamics*.

Cornell, C.A., 1969. Engineering seismic risk analysis. *Bulletin of the Seismological Society of America*, 58(5), 1583-1606.

Cornell, C.A., Krawinkler, H., 2000. Progress and challenges in seismic performance assessment. *PEER Center News*, 3(2), http://peer.berkeley.edu/news/2000spring/index.html

Cornell, C.A., Jalayer, F., Hamburger, R.O., Foutch, D.A., 2002. Probabilistic basis for 2000 SAC Federal Emergency Management Agency steel moment frame guidelines. *Journal of Structural Engineering*, ASCE, 128(4), 526-533.

Esteva, L., Ruiz, S.E., 1989. Seismic failure rates of multistory frames. *Journal of Structural Engineering*, ASCE, 115(2), 268-284.

Hose, Y.D., Seible, F., 1999. Performance evaluation database for concrete bridge components and systems under simulated seismic loads. *Report PEER 1999/11*, Pacific Earthquake Engineering Research Center, University of California at Berkeley, Berkeley, CA.

Idriss, I.M., Sun, J.I, 1993. User's manual for SHAKE91: a computer program for conducting equivalent linear seismic response analyses of horizontally layered soil deposits. *Center for geotechnical modeling*, Dept. of Civil and Environmental Engineering, Univ. of California, Davis, Calfornia.

Kennedy, R.P., Cornell, C.A., Campbell, R.D., Kaplan, S., Perla, H.F., 1980. Probabilistic seismic safety study of an existing nuclear power plant. *Nuclear Engineering and Design*, 59(2), 315-338.

Kramer, S.L., 1996. *Geotechnical earthquake engineering*. Prentice Hall, Upper Saddle River, New Jersey, USA.

Luco, N., Cornell, C.A., 2006. Structure-specific scalar intensity measures for near-source and ordinary earthquake ground motions. *Earthquake Spectra*, under review.

Mazzoni, S., McKenna, F., Fenves, G.L., 2005. *OpenSees: Command Language Manual*. PEER Center, University of California, Berkeley, http://opensees.berkeley.edu/.

Megally, S.H., Silva, P.F., Seible, F., 2001. Seismic response of sacrificial shear keys in bridge abutments. *Report SSRP-2001/23*, University of California, San Diego.

Melek, M., Wallace, J.W., Conte, J.P., 2003. Experimental assessment of columns with short lap splices subjected to cyclic loads. *Report PEER 2003/04*, Pacific Earthquake Engineering Research Center, University of California at Berkeley, Berkeley, CA.

Moehle, J., Deierlein, G.G., 2004. A framework methodology for performance-based earthquake engineering. *Proc. 13th Conf. on Earthquake Eng.*, Vancouver, Canada, 1-6 August.

Nataf, A., 1962. Détermination des distributions dont les marges sont données. *Comptes Rendus de l'Académie des Sciences*, Paris, 225, 42-43.

Porter, K.A., 2003. An overview of PEER's performance-based earthquake engineering methodology. *Proc. of the 9th Int. Conf. on Applic. of Statistics and Probability* (ICASP9) in Civil Eng., Der Kiureghian, A. et al. (eds), San Francisco, California, Vol. 2, 973-980.

Shome, N., Cornell, C.A., Bazzurro, P., Carballo, J.E., 1998. Earthquakes, records, and nonlinear MDOF responses. *Earthquake Spectra*, 14(3), 469-500.

Somerville, P.G., Collins, N., 2002. Ground motion time histories for the Humboldt Bay Bridge. *Report of the PEER Performance Based Earthquake Engineering Methodology Testbed Program*, PEER Center, University of California at Berkeley, Berkeley, CA.

Song, J., Ellingwood, B.R., 1999. Seismic reliability of special moment steel frames with welded connections: II. *Journal of Structural Engineering*, ASCE, 125(4), 372-384.

Tzavelis, C., Shinozuka, M., 1988. Seismic reliability of rigid frames. *Journal of Engineering Mechanics*, ASCE, 114(11), 1953-1972.

Wen, Y.K., 1995. Building reliability and code calibration. *Earthquake Spectra*, 11(2), 269-296.

Yun, S.Y., Hamburger, R.O., Cornell, C.A., Foutch, D.A., 2002. Seismic performance evaluation for steel moment frames. *Journal of Structural Engineering*, ASCE, 128(4), 534-545.

Zhang, Y., Conte, J.P., Yang, Z., Elgamal, A., Bielak, J., Acero, G., 2007a. Two-Dimensional Nonlinear Earthquake Response Analysis of a Bridge-Foundation-Ground System. *Earthquake Spectra*, accepted for publication.

Zhang, Y., Conte, J.P., Acero, G., Somerville, P.G., 2007b. Seismic reliability analysis of a bridge-foundation-ground system: I. with deterministic system properties. In preparation for submission to the *Journal of Structural Engineering*, ASCE.

Zhang, Y., Conte, J.P., 2007c. Seismic reliability analysis of a bridge-foundation-ground system: I. with random system properties. In preparation for submission to the *Journal of Structural Engineering*, ASCE.

Hamburger, R.O., 2004. Development of next-generation performance-based seismic design guidelines. *International Workshop on Performance based seismic design Concepts and implementations*. Bled, Slovenia.

Madsen, H.O., Krenk, S., Lind, N.C., 1986, *Methods of structural sfety*, Prentice-Hall, Inc., Englewood Cliffs, NJ 07632.

Megally, S.H., Silva, P.F., Seible, F., 2001. Seismic response of sacrificial shear keys in bridge abutments. *Report SSRP-2001/23*, University of California at San Diego, La Jolla, CA.